Therapeutic TNF Inhibitors Exhibit Differential Levels of Efficacy in Accelerating Cutaneous Wound Healing

Yonghao Cao[1], Bohdan P. Harvey[1], Liang Jin[2], Susan Westmoreland[3], Jing Wang[4], Munish Puri[3,7], Yingli Yang[3], Holly M. Robb[5,7], Sultan Tanriverdi[1,7], Chenqi Hu[2,7], Xue Wang[2], Xiaofeng Xin[6,7], Yingchun Liu[4,7], Michael P. Macoritto[4], Kathleen M. Smith[4], Yu Tian[2], Kevin White[1], Timothy R.D.J. Radstake[1] and Zehra Kaymakcalan[1]

Adalimumab but neither etanercept nor certolizumab-pegol has been reported to induce a wound-healing profile in vitro by regulating macrophage differentiation and matrix metalloproteinase expression, which may underlie the differences in efficacy between various TNF-α inhibitors in impaired wound healing in patients with hidradenitis suppurativa, a chronic inflammatory skin disease. To examine and compare the efficacy of various TNF inhibitors in cutaneous wound healing in vivo, a human TNF knock-in Lepr$^{db/db}$ mouse model was established to model the impaired cutaneous wound healing as seen in hidradenitis suppurativa. The vehicle group exhibited severe impairments in cutaneous wound healing. In contrast, adalimumab significantly accelerated healing, confirmed by both histologic assessment and a unique healing transcriptional profile. Moreover, adalimumab and infliximab showed similar levels of efficacy, but golimumab was less effective, along with etanercept and certolizumab-pegol. In line with histologic assessments, proteomics analyses from healing wounds exposed to various TNF inhibitors revealed distinct and differential wound-healing signatures that may underlie the differential efficacy of these inhibitors in accelerating cutaneous wound healing. Taken together, these data revealed that TNF inhibitors exhibited differential levels of efficacy in accelerating cutaneous wound healing in the impaired wound-healing model in vivo.

Keywords: Hidradenitis suppurativa, TNF inhibitors, Wound healing

JID Innovations (2024);**4:**100250 doi:10.1016/j.xjidi.2023.100250

INTRODUCTION

Wound healing is an essential physiologic process of tissue repair and regeneration, progressing through sequential stages of hemostasis, inflammation, proliferation, and remodeling in an orderly and timely manner (Gurtner et al, 2008). It consists of a sequence of molecular and cellular events such as soluble mediator secretion, immune cell infiltration, epithelial cell proliferation, and extracellular matrix remodeling (Eming et al, 2007; Rodrigues et al, 2019). Wound healing occurs immediately after tissue injury, starting with platelet activation and degranulation that trigger the inflammatory phase of healing. Transition from the inflammatory to the proliferative phase represents a key step during wound healing (Murray and Wynn, 2011). However, persistent inflammation or infection leads to substantial tissue damage, chronic lesions, and open wounds as seen in diabetic foot ulcers (Theocharidis et al, 2022) as well as patients with hidradenitis suppurativa (HS), a chronic recurrent inflammatory skin disease (Coates et al, 2019; Gierek et al, 2023; Sabat et al, 2020).

Adalimumab (ADA) is the only approved anti−TNF-α inhibitor for the treatment of moderate-to-severe HS (Gupta and Studholme, 2016; Kimball et al, 2016; Zouboulis et al, 2019). In contrast, etanercept (ETN) and certolizumab-pegol (CZP) have been shown ineffective in HS clinical studies (Adams et al, 2010; Lim and Oon, 2019; Maarouf et al, 2018; Sand and Thomsen, 2015; Savage et al, 2019), suggesting that the mechanism of action of ADA is distinct in HS and may contribute to improved wound healing. A previous study has shown that ADA but neither ETN nor CZP induces a wound-healing profile in vitro by regulating macrophage differentiation and matrix metalloproteinase expression, which may underlie the difference in efficacy among various anti−TNF-α agents in impaired wound healing (Cao et al, 2021). Although several studies have suggested that ADA can have a substantial positive impact on HS excisional wound healing

[1]*Transformational and Translational Immunology Discovery, AbbVie Bioresearch Center, Worcester, Massachusetts, USA;* [2]*DMPK-BA, AbbVie Bioresearch Center, Worcester, Massachusetts, USA;* [3]*Phamacology and Pathology, AbbVie Bioresearch Center, Worcester, Massachusetts, USA;* [4]*Immunology Computational Biology, AbbVie Cambridge Research Center, Cambridge, Massachusetts, USA;* [5]*Discovery Research, AbbVie, North Chicago, Illinois, USA; and* [6]*Global Biologics, AbbVie Bioresearch Center, Worcester, Massachusetts, USA*

[7]*Former AbbVie Employee.*

Correspondence: Yonghao Cao, Transformational and Translational Immunology Discovery, AbbVie Bioresearch Center, 100 Research Drive, Worcester, Massachusetts 01605, USA. E-mail: yonghao.cao@abbvie.com

Abbreviations: ADA, adalimumab; CZP, certolizumab-pegol; ETN, etanercept; GOL, golimumab; HS, hidradenitis suppurativa; IFX, infliximab; PSR, Picrosirius red

Received 13 February 2023; revised 21 October 2023; accepted 16 November 2023; accepted manuscript published online XXX; corrected proof published online XXX

Cite this article as: JID Innovations 2024;4:100250

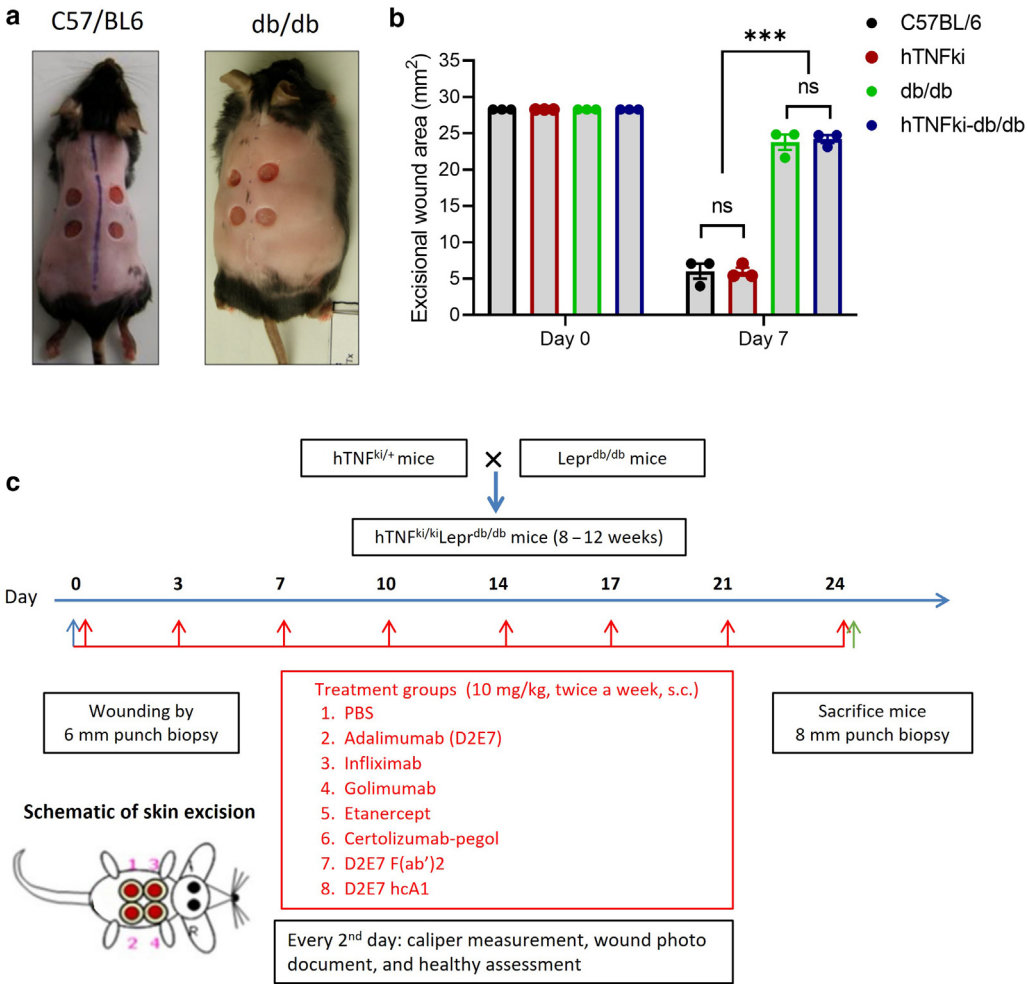

Figure 1. Murine models of acute and impaired cutaneous wound healing. (**a**) Murine models were developed for studying acute and impaired cutaneous wound healing. Four 6-mm full-thickness skin punches were created on the back of the C57BL/6 or db/db mice. (**b**) Excisional wound sizes were evaluated by caliper measurement on C57BL/6, hTNFki, db/db, or hTNFki-db/db mice at baseline and day 7. The results represent the means of wound size from each mouse. ***$P < .001$ (unpaired *t*-test); n = 3 mice per group from 1 of 3 representative studies. (**c**) Schematic representation of the murine model for studying impaired cutaneous wound healing. ns, not significant.

and skin manifestations (Saint-Georges et al, 2018; Zagaria et al, 2020), wound healing and secondary wound reconstruction were not assessed in the SHARPS study (Bechara et al, 2021). In addition to HS, it has been reported in case studies that anti—TNF-α agents may reduce ulcerated necrobiosis lipoidica plaques in patients with type 2 diabetes (Sandhu and Alavi, 2019). The roles of ADA as well as other TNF inhibitors in wound healing are still unclear, and we sought to explore the impact of TNF inhibitors on accelerating the wound-healing process in an in vivo model. Although there is no animal model for HS to date, the diabetic Lepr$^{db/db}$ (db/db) mice could potentially serve as a model for the wound-healing aspects seen in diabetic foot ulcers but also in HS owing to the following similarities. First, one quarter of patients with HS carry diabetes, and half of them have metabolic syndrome as seen in db/db mice (Garg et al, 2018; Gold et al, 2014). Second, patients with HS experience chronic lesions and wounds similar to the impaired wound healing observed in db/db mice (Coates et al, 2019). Finally, inflammatory cytokines, including TNF-α, are significantly elevated in the circulation and wounded or lesional skin from patients with HS and in db/db mice (Kelly et al, 2015; Park et al, 2011).

To investigate the role of therapeutic TNF inhibitors in cutaneous wound healing in vivo, we created an impaired cutaneous wound-healing model by breeding diabetic db/db mice with human TNF-α knock-in mice (ie, hTNFki) mice to generate hTNF$^{ki/ki}$Lepr$^{db/db}$ mice (referred to as hTNFki-db/db mice in the remaining parts of this paper), which express human TNF-α in place of murine TNF-α on the db/db background. Interestingly, our data show that therapeutic TNF inhibitors exhibit differential levels of efficacy in accelerating cutaneous wound healing in vivo, providing additional mechanisms of action of ADA in HS.

RESULTS

A murine model to study impaired cutaneous wound healing in vivo

To develop a murine model of impaired cutaneous wound healing, we selected Lepr$^{db/db}$ (db/db) mice, which in addition to developing diabetes exhibit delayed wound healing (Figure 1a and b). As seen on day 7, only ~20% of healing

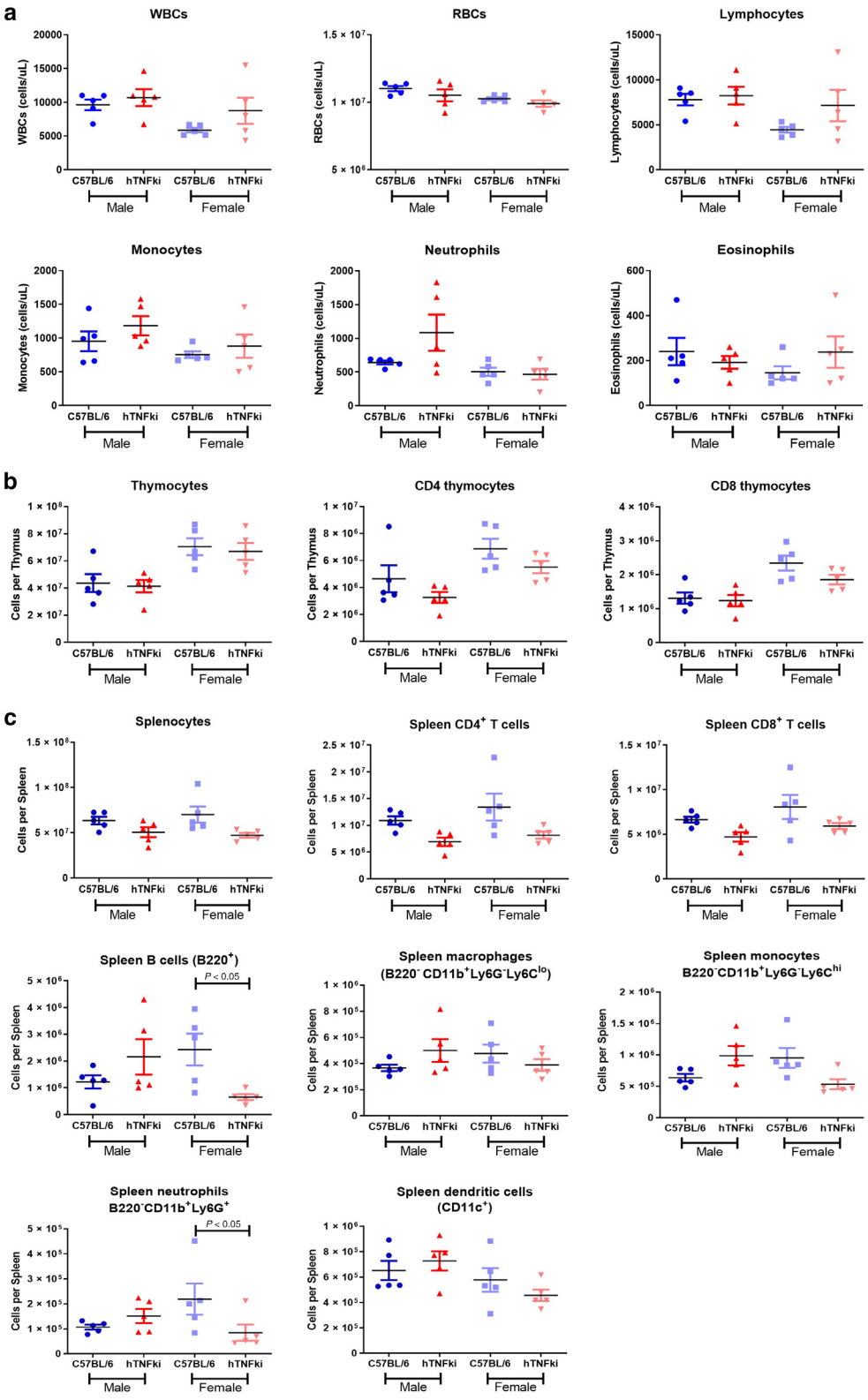

Figure 2. Immunophenotypic analysis in the periphery of hTNFki mice compared with that in C57BL/6 mice. hTNFki and C57BL/6 mice aged 6 weeks were killed to harvest the whole blood, thymus, and spleen samples. Single-cell suspensions were then prepared, and cells were counted and stained for immunophenotypic analysis with the following antibodies against CD4, CD8, B220, CD11b, CD11c, Ly6G, and Ly6C as well as with Zombie. Live single cells were gated and analyzed. (**a**) No significant differences (cell numbers) were observed with WBCs, RBCs, lymphocytes, neutrophils, monocytes, or eosinophils in the blood. (**b**) Minimal differences were observed in the thymus (total thymocyte numbers or CD4 single-positive or CD8 single-positive thymocytes). (**c**) Minimal differences were observed in the spleen, including the total splenocyte numbers, CD4 T cells, CD8 T cells, macrophages, monocytes, or dendritic cells. Slight reduction in B cells and neutrophils in the spleen of hTNFki mice compared with those of C57BL/6 mice but only in females was found. $^*P < .05$, unpaired *t*-test, n = 5 mice per group. Data represent 1 of 2 independent studies. RBC, red blood cell; WBC, white blood cell.

was seen in diabetic (db/db) strains with 6-mm full-thickness excisional wounds, whereas ~80% of wound closure was observed in nondiabetic strains without intervention (Figure 1a–c), supporting that the C57BL/6 mice are more of a model for studying acute wound healing, whereas the db/db mice can be used for studying impaired wound healing.

Because TNF-α is conserved cross-species with 79% homology between human and mouse and shares similar binding affinity and kinetics across murine and human TNF receptors (Butler et al, 1997; Smith et al, 1986), minimal differences in immune phenotypes in the periphery were observed between C57BL/6 and hTNFki mice (Figure 2) as

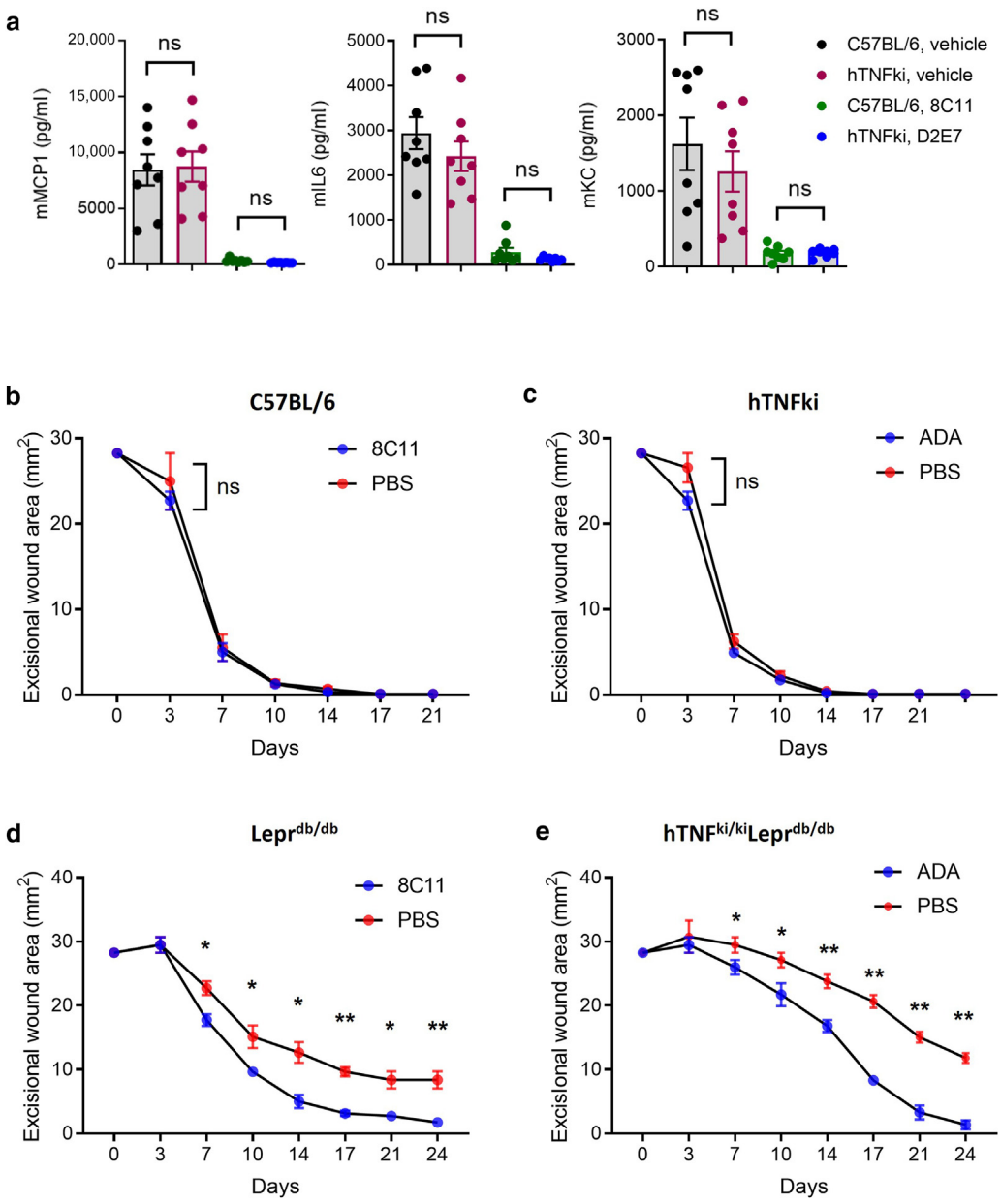

Figure 3. Comparison between acute and impaired wound-healing models. (**a**) Evaluation of C57BL/6 mice and hTNFki mice response to R848. C57BL/6 or hTNFki mice were administered with 8C11 (an anti-mouse TNF-α antibody) or ADA, respectively, for 1 hour, followed by the administration of R848 (15 μg). Peripheral blood was taken after 2 hours of stimulation and tested for murine MCP-1, IL-6, and KC levels in the circulation of C57BL/6 or hTNFki mice in response to 8C11 or ADA, respectively. n = 8 mice per group from 1 of 2 representative studies. Four 6-mm full-thickness excisional wounds were created on the back of indicated mouse strains (**b**) C57BL/6, (**c**) hTNFki, (**d**) db/db, and (**e**) hTNFki-db/db followed by the administration of either ADA (hTNFki and hTNFki-db/db mice) or 8C11 (C57BL/6 and db/db mice) at 20 mg/kg or PBS (vehicle control), twice a week by subcutaneous injection. Wound area measurements and photographs were taken to assess wound size reduction. The results represent the means of wound size from each mouse on the indicated days. $^{*}P < .05$ and $^{**}P < .01$, unpaired *t*-test; n = 3 mice per group from 1 of 3 representative studies. Data represents 2 independent studies. ADA, adalimumab; KC, keratinocyte chemoattractant; MCP-1, monocyte chemoattractant protein-1; ns, not significant.

well as cytokine and chemokine expression, including monocyte chemoattractant protein-1, IL-6, and keratinocyte chemoattractant in response to inflammatory stimuli R848 (Figure 3a). To study the role of TNF inhibitors in impaired cutaneous wound healing, we created a murine cutaneous wound healing model by breeding hTNFki mice with diabetic Lepr$^{db/+}$ mice to generate homozygous hTNFki-db/db mice. Four identical skin excisional wounds were created on the back of hTNFki-db/db mice, followed by administration of either TNF inhibitors or vehicle control (PBS) by subcutaneous injection as indicated in corresponding studies. Wound-healing parameters were assessed during the healing process (Figure 1c).

We first compared wound-healing rates between nondiabetic strains (C57BL/6 and hTNFki) and diabetic strains (db/db and hTNFki-db/db) till day 21 or 24 after injury. Four 6-mm full-thickness excisional wounds were created on the back of these mice, followed by administration of either 8C11 (an anti-mouse TNF-α antibody) or ADA depending on the species of TNF that the strain carried. Wound closure was

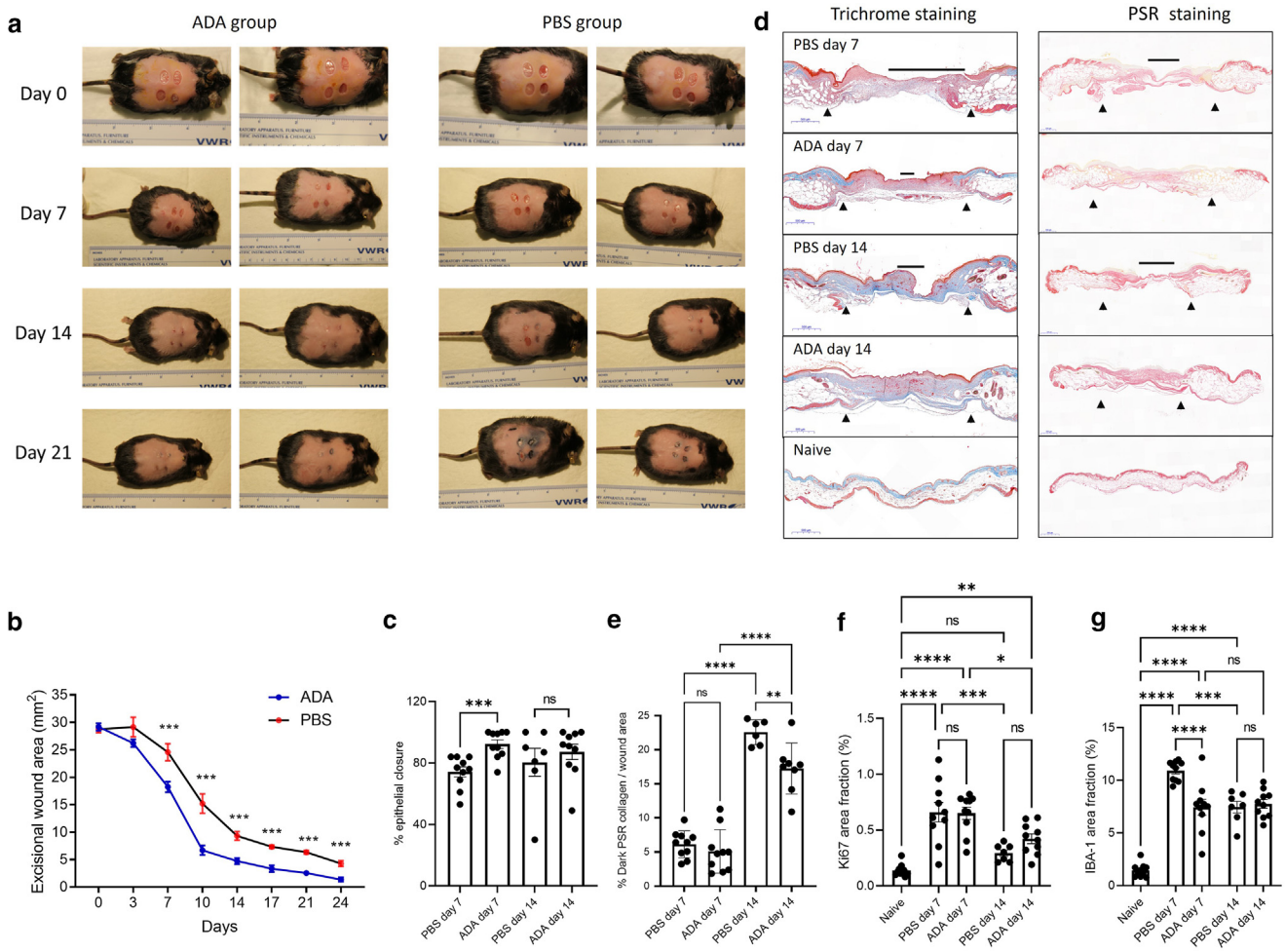

Figure 4. ADA accelerates excisional cutaneous wound healing in hTNFki-db/db mice. (**a**) Four 6-mm full-thickness excisional wounds were created on the back of hTNFki-db/db mice, followed by administration of either ADA (20 mg/kg) or PBS (vehicle control), twice a week by subcutaneous injection. Wound area measurements and photographs were taken to assess wound size reduction. Two representative mice from each group were shown. (**b**) Excisional wound sizes were shown on hTNFki-db/db mice administered with either ADA or PBS (n = 6 mice per group). Results represent 1 of 4 independent experiments. (**c**) Trichrome slides were scanned and measured with a micrometer for epidermal wound length. Epithelial closure was calculated by the percentage of original opening subtracted from 100 and then converted to the percentage of epidermal closure (percentage healed). (**d**) Representative images of trichrome-stained and PSR-stained histologic sections demonstrate epidermal regeneration and collagen deposition at days 7 and 14 after wounding (bar = 500 μm). The edges of the wound are designated by the arrows. The wound area with incomplete re-epithelialization is designated by the thick black line. (**e**) Image analysis quantitation of new (light) versus mature (dark) collagen was performed on PSR slides with VisioPharm. (**f**) Ki-67 staining was quantified to determine the percentage of Ki-67−positive area per section. (**g**) IBA-1 staining was quantified to determine the percentage of IBA-1−positive area per section. Each dot represents the mean readout of 2−4 slides from the same mice. All data are shown as mean ± SEM; n = 10 mice per group from 2 independent studies. *$P < .05$, **$P < .01$, ***$P < .0001$, and ****$P < .0001$; Tukey's multiple comparisons test. ADA, adalimumab; ns, not significant; PSR, Picrosirius red.

fast, mainly in the first week on the nondiabetic strains, regardless of 8C11 or ADA administration (Figure 3b and c). In contrast, wound-healing rate was greatly impaired in both db/db strains, and administration of 8C11 or ADA showed an improvement in wound resolution at similar rates (Figure 3d and e), suggesting that hTNFki-db/db mice are a good model for studying and comparing TNF inhibitors in impaired cutaneous wound healing. Db/db background allows us to study delayed wound healing, whereas the hTNFki gives us the opportunity to compare the efficacy of different TNF inhibitors.

ADA accelerates cutaneous wound healing by improving epidermal closure and tissue granulation

ADA but neither ETN nor CZP induces a profile resembling enhanced wound healing in vitro (Cao et al, 2021). In this study, we first tested whether ADA could significantly promote excisional wound healing in hTNFki-db/db mice. Four 6-mm full-thickness excisional wounds were created on the back of hTNFki-db/db mice, followed by administration of either ADA or vehicle control. Wound area measurements and photographs were taken to document and assess wound size reduction. The vehicle group exhibited a significant delay in cutaneous wound healing at days 7 through 24 after injury compared with the ADA-treated group (Figure 4a and b).

To further examine wound healing, secondary 8-mm punches overlaying the original wounds were created on day 7 or day 14 for histologic assessment. Micrometer-measured epidermal wound diameter length demonstrated smaller open wounds at day 7 in mice administrated with ADA (mean diameter = 470 um) than in those with vehicle control (mean diameter = 1550 um). Then, the data were converted to the rate

of epithelialization, also referred to as the percentage of epithelial closure (Figure 4c). The quality of the wound healing was assessed by quantification of collagen fibers in Picrosirius red (PSR)—stained slides on the basis of color intensity. We quantified new collagen fibers (light PSR), dense fibers (dark PSR), and total fibers (light and dark PSR) as the percentage of wound area. Collagen formation increased significantly in all categories between days 7 and 14 in both groups (Figure 4d). Areas of new collagen at days 7 and 14 were the same across all groups. However, a significantly lower area of mature collagen on day 14 in mice in the ADA-treated group likely represents faster maturation of deposited collagen than that in the vehicle control group (Figure 4d and e).

To assess proliferation, we quantified Ki-67—stained cells as a percentage of the total area demonstrating a robust significant increase in proliferation in both PBS- and ADA-treated groups on day 7 compared with that at baseline (naïve group on day 0), which was maintained in the ADA-treated group only on day 14 (Figure 4f). Finally, to assess wound-healing—associated inflammation, we stained slides with the pan-myeloid marker IBA-1, which was overall increased above naïve in both ADA- and PBS-treated groups at days 7 and 14. Administration of ADA significantly reduced IBA-1 expression in healing wounds on day 7 compared with that in the control group but not on day 14, suggesting that early wound-healing—associated inflammation is partially TNF driven (Figure 4g).

Distinct wound-healing signatures in mice treated with ADA

The wound-healing data, described earlier, showed that ADA accelerated cutaneous wound healing in hTNFki-db/db mice. To understand the molecular mechanisms that underlie the role of ADA in promoting cutaneous wound healing, secondary 8-mm excisional punches were created around healing wounds. RNA sequencing was performed on perilesional skin biopsies at baseline and on days 3, 7, and 10. We identified differentially expressed genes in healing wounds of mice administrated with either ADA or vehicle control compared with their baseline, respectively (Figure 5a and b and Supplementary Table S1). Heatmaps of the differentially expressed genes suggested distinct gene profiles in the 2 treatment groups. Moreover, canonical pathway analysis revealed a distinct wound-healing signature from wounded skin exposed to ADA, including hepatic fibrosis signaling that involves genes associated with tissue repair such as collagens, TGF-β, and GFs. Immune infiltration and inflammatory pathways (eg, granulocyte and agranulocyte adhesion and diapedesis pathways) were enriched in both treatment groups through day 10 (Figure 5c and Supplementary Table S2), with most being represented at a higher level in the ADA-treated group. Many of the inflammation-associated pathways consist of genes (Supplementary Table S2) commonly expressed by fibroblasts, keratinocytes, and endothelial cells, and these cells are known to be directly involved in tissue repair, suggesting that exposure to ADA is enhancing the influx of cells involved in wound healing. In addition, TREM1 signaling and IL-8 signaling, known to promote neutrophil extracellular trap formation and diabetic wound healing (Rennekampff et al, 2000; Sawaya et al, 2022), were upregulated in wounded skin administrated with ADA. Interestingly, RNA sequencing of perilesional skin biopsies from ADA-treated mice revealed a wound-healing signature similar to that reported previously with inflammatory human macrophages (Cao et al, 2021), including inhibition of matrix metalloproteinase signaling as well as promotion of wound healing signaling pathway, HIF-1 signaling, and Fcγ receptor—mediated phagocytosis (Figure 5c and Supplementary Table S2). In conclusion, our data demonstrate that ADA accelerates cutaneous wound healing in vivo by inducing a distinct healing signature.

Different TNF inhibitors exhibit distinct levels of efficacy in accelerating cutaneous wound healing

Unlike ADA, ETN and CZP are ineffective in clinical studies of HS (Adams et al, 2010; Lim and Oon, 2019; Maarouf et al, 2018; Savage et al, 2019). To understand the mechanism of action of the various TNF inhibitors in accelerating wound healing, we compared their efficacies in the impaired cutaneous wound healing model as described earlier. Four identical 6-mm wounds were created on the back of hTNFki-db/db mice, followed by the administration of various anti-TNF inhibitors. As shown in Figure 6a, ADA and infliximab (IFX) were more effective and showed similar levels of efficacy starting from day 7 and throughout the healing process. In contrast, golimumab (GOL) along with ETN and CZP was less effective and not significantly different from that of the vehicle control group on day 21 (Figure 6b). Because ETN and CZP do not have functional Fc (fragment crystallizable) domains, the 2 TNF inhibitors cannot form large TNF—anti-TNF complexes as ADA does (Santora et al, 2001). We then explored 2 modified formats of ADA: D2E7 F(ab')2 (F(ab')2 fragments of ADA) and D2E7-hcA1 (an IgA1 Fc-domain type of ADA). Interestingly, neither D2E7 F(ab')2 nor D2E7-hcA1 showed significant efficacy in accelerating cutaneous wound healing in hTNFki-db/db mice (Figure 6a and b), suggesting the critical role of the Fc domain and potentially the large immunological complexes that may form in vivo in contributing to the accelerated healing of cutaneous wounds.

Proteomics analysis reveals distinct molecular signatures associated with wound healing in mice treated with TNF inhibitors

To understand the mechanisms underlying the different efficacies of TNF inhibitors in impaired wound healing, we performed liquid chromatography—mass spectrometry—based label-free proteomics studies on wounded skin exposed to various TNF inhibitors or vehicle control. Secondary 8-mm excisional punches were created around healing wounds on day 3 and day 10 for proteomics analysis. Principal component analysis revealed no clear separation between each treatment on day 3 (Figure 7a). Consistent with the principal component analysis result, no clear differentially expressed proteins (Figure 7b and Supplementary Table S3) or pathways were identified from each treatment group on day 3 (Figure 7c), suggesting that wound healing had not yet transited into proliferation and remodeling stages.

On day 10, the principal component analysis result showed that the vehicle control (PBS) group clustered in the middle; ADA, IFX, and D2E7 F(ab')2 groups clustered together to the far left of the plot, whereas GOL, ETN and

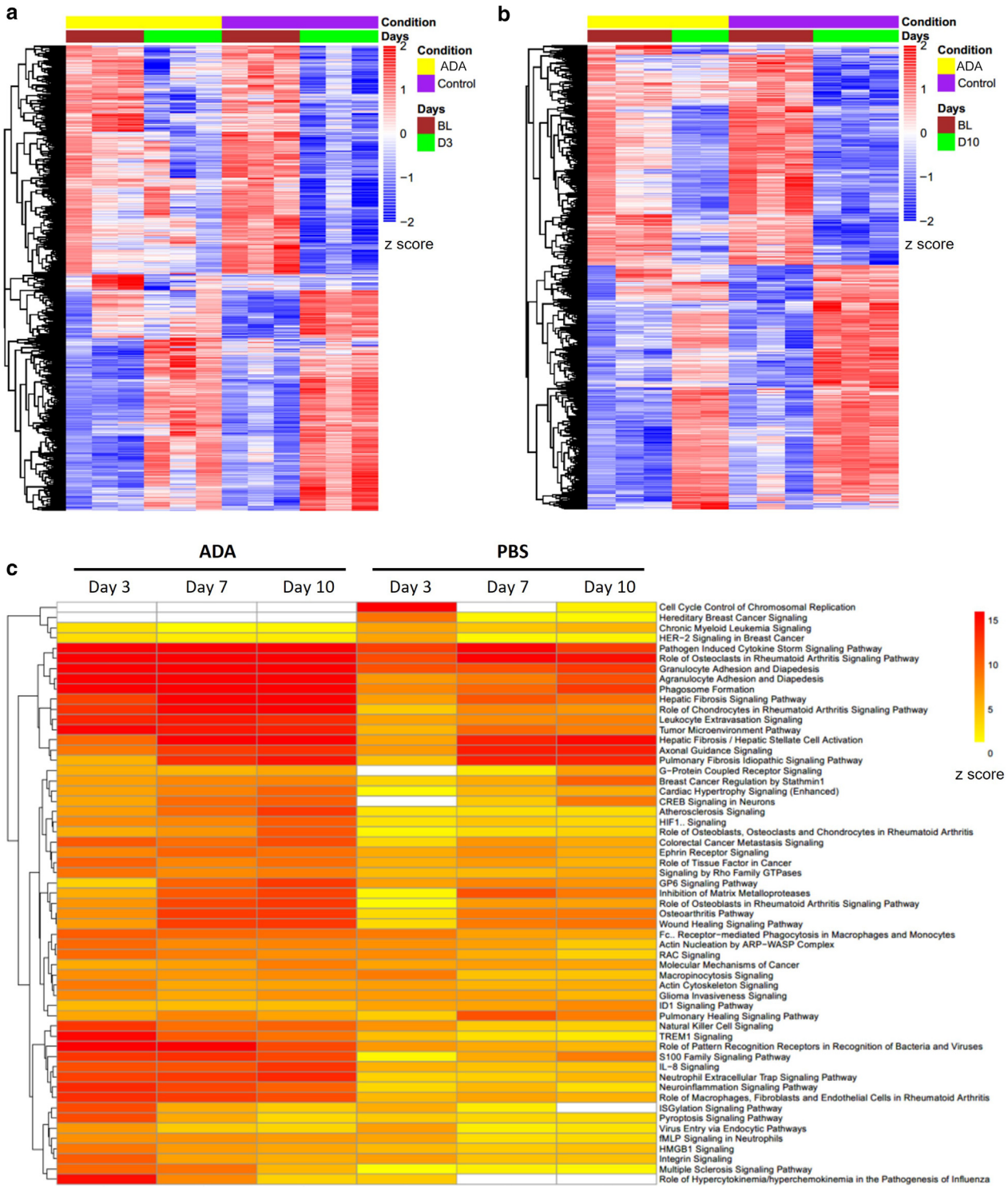

Figure 5. Differentially expressed genes and pathways in wounded skin after ADA or vehicle control administration. Four 6-mm full-thickness excisional wounds were created on the back of hTNFki-db/db mice, followed by administration of either ADA (20 mg/kg) or vehicle control, twice a week by subcutaneous injection. Wounded skin tissues from each group were collected on days 0 (baseline), 3, 7, and 10 for RNA sequencing. Data show the differentially expressed genes (fold change ≥ 2; FDR < 0.05) from wounded skin samples exposed to either ADA or vehicle control compared with that at its baseline at (**a**) day 3 or (**b**) day 10. (**c**) Enriched pathways in wounded skin exposed to ADA or vehicle control by IPA. The differentially expressed genes were used for IPA. The heatmap shows the top 30 canonical enriched pathways (FDR < 0.05) from each treatment group on days 3, 7, and 10 compared with those at their baselines. White in the heatmap represents FDR < 0.05. For the color gradient of each heatmap, data were transformed by $\log_2$ for the logarithmic function and normalized by z score, which was defined by the mean expression of each gene across all samples divided by its SD. BL denotes baseline, and D10 denotes day 10. ADA, adalimumab; FDR, false discovery rate; IPA, Ingenuity Pathway Analysis.

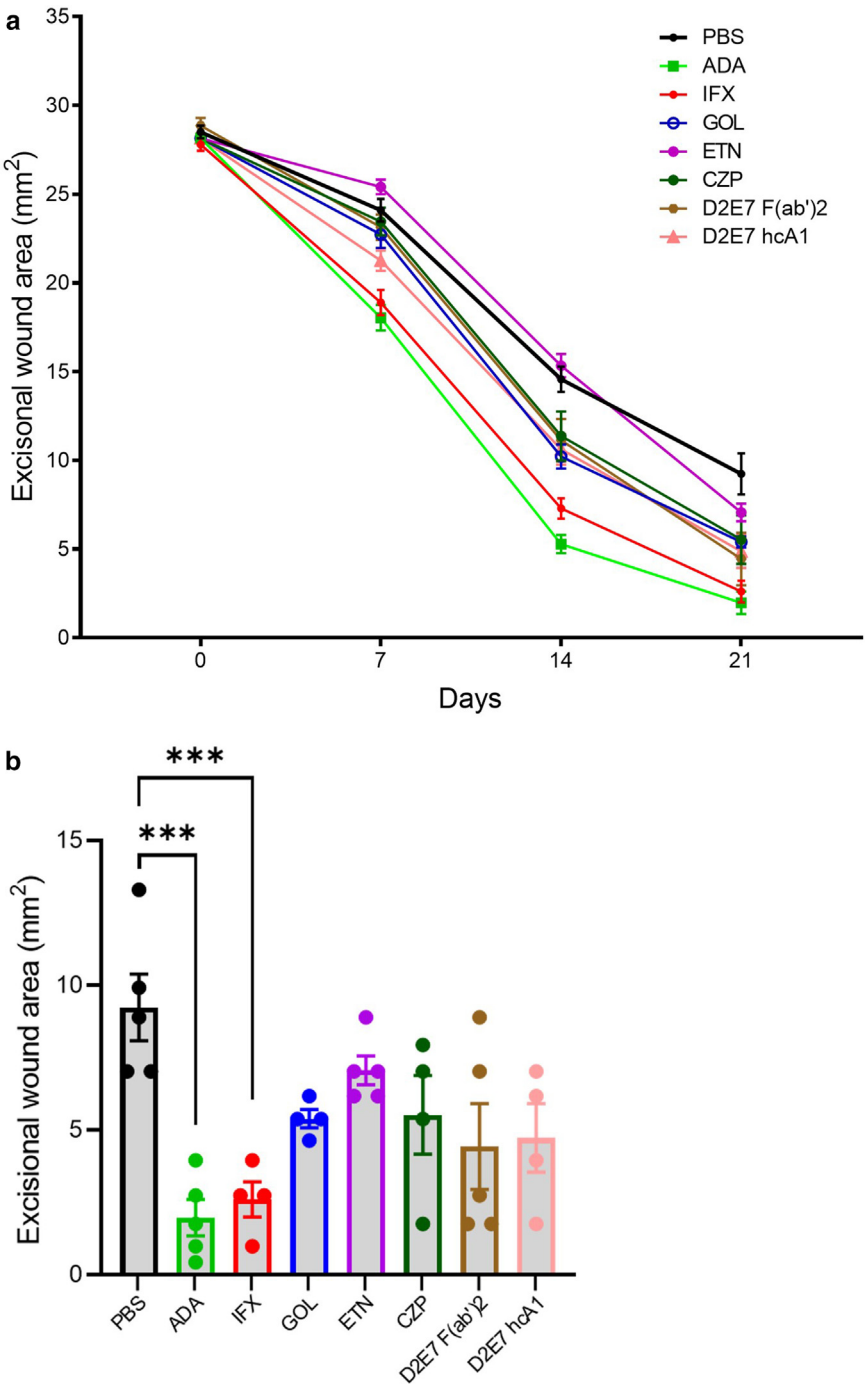

Figure 6. TNF inhibitors exhibit differential levels of efficacy in accelerating cutaneous wound healing in vivo. (**a**) Four identical 6-mm skin punch wounds were created on the back of homozygous hTNFki-db/db experimental mice, followed by administration of either each TNF inhibitor (10 mg/kg) or vehicle control (PBS), twice a week by subcutaneous injection. (**a**) The size of excision wounds was measured and calculated. Data are shown as mean ± SEM (each error bar is constructed using 1 SEM). **(b)** Wound healing at day 21 for each treatment group. The results represent the means of wound size from each mouse. ***$P < .001$ (unpaired *t*-test); n = 5 mice per group. Results represent 1 of 4 independent studies. ADA, adalimumab; ETN, etanercept; GOL, golimumab; IFX, infliximab.

CZP groups clustered more to the right (Figure 7a). Heatmap of differentially expressed proteins revealed similar protein expression patterns on healing wounds that were exposed to ADA, IFX, and D2E7 F(ab')2. In contrast, GOL, ETN, and CZP groups exhibited similar protein expression patterns, resembling those of the vehicle control group (Figure 7b and Supplementary Table S3). Then, pathway over-representation analysis with Ontology (Gene Ontology) terms of biological processes was performed on differentially expressed proteins of each treatment group compared with those in the vehicle control group on day 10. Selected pathways related to wound healing are presented in Figure 7c. Most interestingly, ADA- and IFX-treated groups, along with D2E7 F(ab')2—treated groups, exhibited distinct proliferation/remodeling stage-related pathways, including enhanced filament-based process and organization, muscle cell differentiation, and muscle tissue development, each being reported as critical events during wound healing (Abreu-Blanco et al, 2012; Huard et al, 2002; Rodrigues et al, 2019). Notably, response to wounding pathway was identified only in ADA- and IFX-treated groups. Moreover, the ADA-treated group exhibited unique healing pathways, similar to skin development, semaphorin—plexin

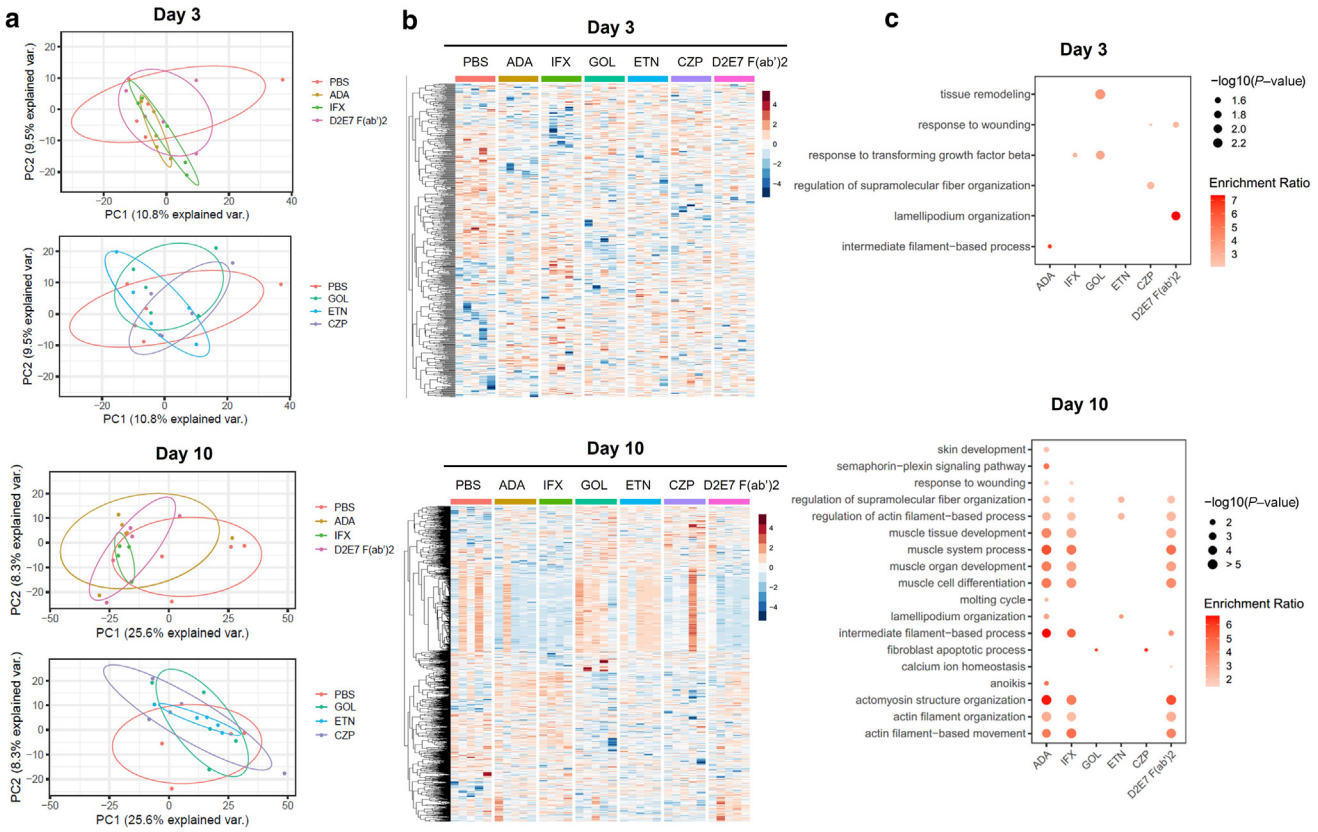

Figure 7. Differential expression proteins and enriched pathways in healing wounds exposed to various TNF inhibitors. Principal component analysis of correlations and variations of protein profiles from healing wounds exposed to TNF inhibitors on (**a**) day 3 and day 10. Heatmap shows DEPs identified by proteomics from healing skin exposed to indicated TNF inhibitors or vehicle control (PBS) on (**b**) day 3 and day 10. DEPs were defined with $P < .05$ and fold change > 1.5 in the pairwise comparisons. Pathway over-representation analysis with Ontology (GO) terms of biological processes was performed with DEPs from healing skin exposed to indicated TNF inhibitors compared with that of the vehicle control on (**c**) day 3 and day 10. Pathways with $P < .05$ were shown in at least 1 comparison group. The statistical significance of pathway over-representation was indicated by the dot size, and the ratio of enrichment was indicated by the color scales. n = 5 mice per group. D2E7 F(ab')2 denotes F(ab')2 fragments of ADA; D2E7-hCa1 denotes IgA1 Fc-type of ADA. ADA, adalimumab; CZP, certolizumab-pegol; DEP, differential expression protein; ETN, etanercept; GO, Gene Ontology; GOL, golimumab; IFX, infliximab; PC1, principal component 1; PC2, principal component 2.

signaling, molting cycle, and anoikis (Figure 7c), which have been identified as key pathways that promote wound healing (Takeo et al, 2015; Xia et al, 2015). In contrast, a few pathways linked to filament-based process and organization were enriched in the ETN-treated group, and fibroblast apoptotic process was the only pathway showing in CZP- and GOL-treated groups, which may help explain the differences observed with each TNF inhibitor regarding its impact on cutaneous wound healing.

DISCUSSION

Previous study has reported that the TNF inhibitor ADA but neither ETN nor CZP induces a wound-healing profile in vitro by regulating macrophage differentiation and matrix metalloproteinase expression in patients with HS (Cao et al, 2021). In this study, we have demonstrated that various TNF inhibitors exhibited different levels of efficacy in accelerating cutaneous wound healing in an in vivo mouse model, which may provide additional mechanism of action insights of TNF inhibitors in autoimmune-related skin disorders as observed in HS and diabetes.

Wound healing is achieved through programmed phases of hemostasis, inflammation, proliferation, and remodeling in a sequential and temporal manner. Chronically delayed wound healing occurs owing to excessive and persistent inflammation, as seen in HS and diabetes and is modeled in db/db mice (Krzyszczyk et al, 2018; Larouche et al, 2018). In this study, RNA sequencing revealed that ADA accelerates cutaneous wound healing on the basis of enrichment in pathways associated with the influx and phenotypic properties of cells involved in tissue repair, including fibroblasts, keratinocytes, and endothelial cells, as well as neutrophil extracellular trap formation by TREM1 and IL-8 signaling (Rennekampff et al, 2000; Sawaya et al, 2022). Moreover, histologic assessment supported that ADA accelerates wound closure by day 7, coincident with the reduction in tissue pan-myeloid marker IBA-1. This supports the beneficial role of the anti-inflammatory mechanism of action of ADA in wound healing. More specifically, these findings mirror those that were previously reported in in vitro studies with primary human macrophages that TNF—ADA complexes can induce a wound-healing profile by diverting inflammatory macrophages into a regulatory/healing phenotype (Cao et al, 2021). Further analyses of immune infiltrates would help in understanding the role of these immune cells in ADA-mediated wound healing.

The roles of TNF and TNF inhibitors in wound healing have been difficult to elucidate. In 1 series of studies, TNF was found to promote acute wound healing but to impair chronic wound healing; others reported that chronic wounds benefit from anti-TNF intervention to achieve complete healing (Ashcroft et al, 2012; Ritsu et al, 2017; Sandhu and Alavi, 2019; Theocharidis et al, 2022; Xu et al, 2013; Yan et al, 2010). Our study expands on these earlier reports in that not all TNF inhibitors affect cutaneous wound healing equally.

First, proteomics analysis indicated that healing wounds exposed to ADA and IFX but not other TNF inhibitors exhibited distinct tissue remodeling–related pathways on day 10. Transcriptomics data provide an overview of global gene expression, indicating that there is a delayed transition at the inflammatory phase. In concordance with the transcriptomics findings, the proteomics data show that the quality of wound healing is improved, indicated by enriched pathways that participate in skin development and tissue remodeling. Second, a functional Fc fragment is required for the transition from the inflammatory stage to the regulatory stage of healing. ETN and CZP, along with D2E7 F(ab')2, showed only partial efficacy in the cutaneous wound healing possibly owing to a lack of functional Fc-receptor engagement. These data also indicate that in addition to mere TNF neutralization, an FcγR-dependent effect may be required, supporting previous in vitro studies (Cao et al, 2021). The accelerated wound healing with ADA and IFX may also be explained by the observation that these 2 drugs exhibit significantly longer drug survival times than ETN in patients with HS (Ring et al, 2022). The lower drug level of ETN has been also observed in our wound-healing study. Third, the absence of large complex formation of ETN, CZP, and D2E7-hcA1 binding to TNF may account for the different clinical efficacy profiles of the TNF antagonists (Contreras et al, 2020). Finally, it remains unclear why GOL failed to improve healing in this model. Indeed, GOL seems to be less effective in inflammatory bowel diseases than ADA and IFX (Mitoma et al, 2018). The way ADA and IFX bind to TNF and form higher-order complexes might contribute to their improved efficacy in certain circumstances (Kohno et al, 2007; Tran et al, 2017). More studies are needed to further elucidate the mechanisms behind this phenotype.

Under the assumption that anti-TNF treatment would result in higher infection rates and delay wound healing, it has been recommended in clinical practice to discontinue anti-TNF drug use before surgery (Moosvi et al, 2020). Depending on the type of procedure performed, postoperative rates of recurrence in patients with HS range as high as 70%. Wide-excision surgery reduces the risk of recurrence, but patients still need postoperative care to address wound healing and minimize infection. Our results provide potential insights into why ADA administration could lead to improved efficacy in conjunction with wide-excision surgery for patients with HS who require surgical intervention as was reported in the HS SHARPS clinical study (Bechara et al, 2021). Additional studies have shown that ADA promotes HS excisional wound healing and skin manifestations (Saint-Georges et al, 2018; Zagaria et al, 2020). Moreover, a pilot study, presented by Gefion Girbig at the 2020 European Academy of Dermatology and Venereology congress, showed that in conjunction with wide-excision surgery, ADA enhances primary wound closure after HS surgery and reduces secondary wound healing disorders and complications. In addition, no increased infection risk was reported in the landmark PUCCINI study (the postoperative infection inflammatory bowel disease trial) nor in the SHARPS study (Bechara et al, 2021; Cohen et al, 2019).

In conclusion, our preclinical data show that TNF inhibitors exhibited different levels of efficacy in accelerating cutaneous wound healing in vivo. An HS model or ex vivo complex model would help further validate the role of TNF inhibitors in impaired wound healing in HS. Additional clinical studies may be required to extend these observations.

MATERIALS AND METHODS

Animals

C57BL/6 mice, hTNF$^{ki/ki}$ mice, and B6.BKS(D)-Leprd$^{b/J}$ mice were purchased from Jackson Laboratories and housed in a specific pathogen-free animal facility. Lepr$^{db/+}$ mice and hTNF$^{ki/+}$ mice were maintained and bred at Jackson Laboratories. Homozygous hTNF$^{ki/ki}$Lepr$^{db/db}$ mice (aged 6 weeks) were purchased, and mice aged 8–12 weeks were used for wound-healing studies. All mice were acclimated in the facility for at least 7 days prior to use, with mice housed 5 per cage on a 12-hour light–dark cycle with food and water provided ad libitum. All animal studies were performed in accordance with and under protocols approved by the AbbVie Bioresearch Center Institutional Animal Care and Use Committee in accordance with the Principles of Laboratory Animal Care and all applicable national and local laws.

Toll-like receptor 7/8 agonist R848 challenge

To study hTNFki mice responding to inflammatory stimuli, C57BL/6 or hTNF$^{ki/ki}$ mice aged 8 weeks were administered by intraperitoneal injection with either vehicle control or anti-TNF antibody (8C11 or D2E7, 15 mpk, respectively) 1 hour before the R848 challenging. The mice were then challenged with toll-like receptor 7/8 agonist R848 (15 μg per mouse by subcutaneous injection). Peripheral blood was taken after 2 hours of challenge to measure the levels of murine monocyte chemoattractant protein-1, IL-6, and keratinocyte chemoattractant in the circulation of C57BL/6 or hTNFki mice by ELISA.

Wound surgery

Wound surgery was performed on the indicated mouse stains as described (Dunn et al, 2013). Mice (aged 8∼12 weeks) were placed in a chamber and anesthetized with 5% isoflurane (VetEquip, Livermore, CA) to prepare the mice. The fur on the dorsal skin was removed with an electric shaver, followed by the application of Nair hair removal cream for no more than 1 minute. The dorsal skin was cleaned and sterilized with iodine solution. After depilation, four 6-mm diameter full-thickness skin punches extending through the panniculus carnosus were made on the dorsa of mice with skin biopsy punches (Acuderm, Fort Lauderdale, FL) and dressed by Tegaderm transparent film. Mice were administrated with tramadol (5 mg/kg, single dose) and indicated TNF inhibitors or vehicle control (twice a week by subcutaneous injection). Wounds were measured by caliper and photographed every other day and visually monitored for possible signs of infection. The wound area was quantified by tracing wound margins and calculated as a percentage of the original wound size, with scaling normalized to the original wound. Secondary 8-mm full-thickness skin punches overlaying the original

wounds were harvested on indicated days for histologic analysis, RNA sequencing, or proteomics studies.

Histology and immunohistochemistry analysis

Four 6-mm wounds were created on the back of hTNFki-db/db mice, followed by administration of either ADA (10 mg/kg, twice a week) or vehicle control. Secondary 8-mm punches overlaying the original wounds were created for histologic assessment at 7 or 10 days after wound surgery. Two samples per mouse were fixed in 10% neutral-buffered formalin, processed, hemisectioned, and embedded in paraffin blocks (4 skin hemisectioned pieces per mouse per block). The tissues were then sectioned at 5 μm and stained with Mason's Trichrome or PSR. All slides were scanned on a Pannoramic 250 Slide Scanner (3D Histech) and visualized using CaseViewer. Trichrome slides were used to quantitatively measure the width of epidermal wound opening for each piece (n = 4 per mouse) using the Caseviewer measuring tool. Data were graphed as an average measurement for persistent opening of the 4 hemisectioned skin samples per mouse. PSR slides were quantitatively assessed with computer image analysis with VisioPharm or collagen deposition and maturation.

Immunohistochemistry was performed to assess myeloid response in wound healing with the pan-myeloid marker IBA1 (Wako, 019-19741) and cellular proliferation with Ki-67 (Roche, 790-4286) using the Leica Bond RX. Mouse skin sections were subjected to EDTA or citrate heat-induced epitope retrieval, respectively. They were incubated with the primary antibodies against IBA1 or Ki-67, detected with Leica's horseradish peroxidase polymer, and visualized with 3, 3′-diaminobenzidine (Leica's Bond Polymer Refine Detection kit) and then counterstained with hematoxylin. The slides were scanned on a Pannoramic 250 Slide Scanner (3D Histech).

RNA sequencing

Transcriptome analyses were carried out on wounded skin exposed to various TNF inhibitors or vehicle control by next-generation RNA sequencing previously described (Cao et al, 2015). Naïve skin samples and 8-mm secondary punches were performed on days 0, 3, 7, and 10. RNA was extracted using the RNeasy Mini Kit (Qiagen, Hilden, Germany) according to the manufacturer's instructions. RNA library preparation from total RNA was conducted, following the manufacturer's instructions, for the SMARTer Stranded Total RNA-Seq Kit V2-Pico (Mountain View, CA). Final libraries were assessed using the Agilent Tapestation and Qubit assay methods (Thermo Fisher Scientific, Waltham, MA) and then sequenced on an Illumina NextSeq500 sequencer using 1 × 50 bp read length for a depth of 50 M reads.

RNA-sequencing data were analyzed as described (Conesa et al, 2016). RNA-sequencing reads were aligned to the mouse genome (GRCm39) with STAR (Dobin et al, 2013). In the count matrix, genes with CPM (counts per million) >1 in less than 20% of all samples were removed for further analyses. Then, the count matrix was normalized on the basis of the TMM (Trimmed Mean of M-values) method (Robinson and Oshlack, 2010) and transformed by logarithmic function. The differentially expressed genes for each comparison were identified on the basis of the Limma method under fold change > 2 and false discovery rate < 0.05 (Ritchie et al, 2015). Pathway analyses were performed using Ingenuity Pathway Analysis (www.ingenuity.com). The differentially expressed genes from each treatment group on days 3, 7, and 10 compared with those at baseline were used as input for Ingenuity Pathway Analysis. The significant upregulated and downregulated canonical pathways were identified under false discovery rate < 0.05.

Proteomics analysis

Secondary 8-mm punches overlaying the original wounds were collected on days 3 and 10. All skin punches were subjected to an extensive, reproducible protein extraction with Bioruptor-assisted sonication and overnight extraction in SDS solubilization buffer. The extracts were then processed following S-Trap mini spin column digestion protocol (ProtiFi). A SWATH DIA label-free proteomics platform (Shen et al, 2023; Wang et al, 2021) was employed for protein identification and quantification. A comprehensive spectral library was built through extensive peptide fractionation by strong anion exchange followed by high-pH reverse-phase high-performance liquid chromatography. The data-dependent acquisition data of the 60 fractions and data-independent acquisition data of 79 experimental samples further generated a hybrid library using Pulsar search engine in Spectronaut (Biognosys). The liquid chromatography instrumentation employed the micro-flow Dionex RSLC 3000 system (Thermo Fisher Scientific) coupled with nanoEase M/Z Peptide CSH C18 Column. The mass spectrometer was calibrated using liquid chromatography–mass spectrometry injection of beta-galactosidase trypsin digest (Sciex) after every 2 sample injections to maintain mass accuracy and resolution. The quantitative SWATH-MS data were analyzed by DIA-NN (Demichev et al, 2020).

Protein identifications with high missingness were filtered on the basis of the satisfaction of at least 1 of 2 criteria: first, proteins should have at least 50% values across all samples, and second, proteins have at least 80% values in samples from any sample group. The overall missing value rate was 28.9% before filtering and 9.03% after filtering. Protein abundances were then normalized using normalizeCyclicLoess function in the limma R package (Ritchie et al, 2015), and missing values were imputed using missForest function from the missForest R package (Stekhoven and Buhlmann, 2012). This random forest–based imputation approach has demonstrated superior accuracy in imputing proteomic data (Jin et al, 2021). The limma R package (Ritchie et al, 2015) was used to perform differential expression analysis. Over-representation analysis of pathways in the differentially expressed proteins was performed using WebGestaltR R package (Liao et al, 2019) against the Gene Ontology terms of biological processes. Protein coding genes were used as the reference set, and all other parameters were kept default.

Ethics statement

All animal studies were performed in accordance with and under protocols approved by the AbbVie Bioresearch Center Institutional Animal Care and Use Committee in accordance with the Principles of Laboratory Animal Care and all applicable national and local laws.

Data availability statement

RNA-sequencing datasets (GSE242837) related to this article have been deposited at https://www.ncbi.nlm.nih.gov/geo/query/acc.cgi?acc=GSE242837, an open-source online data repository hosted at the Gene Expression Omnibus at National Center for Biotechnology Information. The mass spectrometry proteomics data have been deposited at the ProteomeXchange Consortium through the PRIDE partner repository with the dataset identifier PXD040275 (https://www.ebi.ac.uk/pride/archive/projects/PXD040275).

ORCIDs
Yonghao Cao: http://orcid.org/0000-0002-1350-7316
Bohdan P. Harvey: http://orcid.org/0000-0001-8193-9340
Liang Jin: http://orcid.org/0000-0002-8659-0536
Susan Westmoreland: http://orcid.org/0000-0002-0286-5599
Jing Wang: http://orcid.org/0000-0001-9491-4994
Munish Puri: http://orcid.org/0000-0001-6603-4447
Yingli Yang: http://orcid.org/0000-0003-1571-2724
Holly M. Robb: http://orcid.org/0000-0003-3982-4587
Sultan Tanriverdi: http://orcid.org/0000-0002-8695-9559
Chenqi Hu: http://orcid.org/0000-0002-0542-3198
Xue Wang: http://orcid.org/0000-0002-5267-6083
Xiaofeng Xin: http://orcid.org/0000-0002-2439-7183
Yingchun Liu: http://orcid.org/0000-0002-4531-6565
Michael P. Macoritto: https://orcid.org/0000-0002-1858-9867
Kathleen M. Smith: http://orcid.org/0000-0001-7833-3102
Yu Tian: http://orcid.org/0000-0003-3754-5875
Kevin White: http://orcid.org/0000-0002-8082-8494
Timothy R. D. J. Radstake: http://orcid.org/0000-0003-1241-6911
Zehra Kaymakcalan: http://orcid.org/0000-0002-3488-3919

CONFLICT OF INTEREST
YC, BPH, LJ, SW, JW, YY, HMR, XW, MPM, KMS, YT, KW, TRDJR, and ZK are employees of AbbVie. MP, ST, CH, XX, and YL were employees of AbbVie at the time of the study. The design, study conduct, and financial support for this research were provided by AbbVie.

ACKNOWLEDGMENTS
The authors would like to thank AbbVie employees Jochen Salfeld, Stephanie Harbers, and Beth Rycroft for their critical review of these studies and Tyler Vincent, Emily Conti, Paige Benoit, and former AbbVie employee Art Nikkel for their technical support. This study was funded by AbbVie.

AUTHOR CONTRIBUTIONS
Conceptualization: YC, BPH, ZK; Formal Analysis: YC, LJ, SW, JW, MP, YY, HMR, ST, YL, KMS, MPM; Investigation: YC, BPH, LJ, SW, JW, ST, CH, XW, XX, ZK; Methodology: YC, LJ, SW, CH, XW, YT, ZK; Project Administration: YC, ZK; Resources: YC, SW, YT, KW, TRDJR, ZK; Supervision: KW, TRDJR, ZK; Visualization: YC, LJ, SW, YL; Writing - Original Draft Preparation: YC, BPH; Writing – Review and Editing: YC, BPH, LJ, SW, JW, MP, YY, HMR, ST, CH, XW, XX, YL, MPM, KMS, YT, KW, TRDJR, ZK

Disclaimer
AbbVie funded this study and participated in the interpretation of data, review, and approval of the publication. These data are offered for scientific discussion in the context of a better understanding of the complex mechanism of action of therapeutics and their specific clinical data; these data are not intended to suggest the performance of a therapeutic that is not established by clinical investigation and, as appropriate, reviewed by a regulatory agency.

REFERENCES

Abreu-Blanco MT, Watts JJ, Verboon JM, Parkhurst SM. Cytoskeleton responses in wound repair. Cell Mol Life Sci 2012;69:2469–83.

Adams DR, Yankura JA, Fogelberg AC, Anderson BE. Treatment of hidradenitis suppurativa with Etanercept injection. Arch Dermatol 2010;146:501–4.

Ashcroft GS, Jeong MJ, Ashworth JJ, Hardman M, Jin W, Moutsopoulos N, et al. Tumor necrosis factor-alpha (TNF-α) is a therapeutic target for impaired cutaneous wound healing. Wound Repair Regen 2012;20:38–49.

Bechara FG, Podda M, Prens EP, Horváth B, Giamarellos-Bourboulis EJ, Alavi A, et al. Efficacy and safety of adalimumab in conjunction with surgery in moderate to severe hidradenitis suppurativa: the SHARPS randomized clinical trial. JAMA Surg 2021;156:1001–9.

Butler DM, Malfait AM, Mason LJ, Warden PJ, Kollias G, Maini RN, et al. DBA/1 mice expressing the human TNF-alpha transgene develop a severe, erosive arthritis: characterization of the cytokine cascade and cellular composition. J Immunol 1997;159:2867–76.

Cao Y, Goods BA, Raddassi K, Nepom GT, Kwok WW, Love JC, et al. Functional inflammatory profiles distinguish myelin-reactive T cells from patients with multiple sclerosis. Sci Transl Med 2015;7:287ra74.

Cao Y, Harvey BP, Hong F, Ruzek M, Wang J, Murphy ER, et al. Adalimumab induces a wound healing profile in patients with hidradenitis suppurativa by regulating macrophage differentiation and matrix metalloproteinase expression. J Invest Dermatol 2021;141:2730–40.e9.

Coates M, Mariottoni P, Corcoran DL, Kirshner HF, Jaleel T, Brown DA, et al. The skin transcriptome in hidradenitis suppurativa uncovers an antimicrobial and sweat gland gene signature which has distinct overlap with wounded skin. PLoS One 2019;14:e0216249.

Cohen BL, Fleshner P, Kane SV, Herfarth HH, Palekar N, Farraye FA, et al. Anti-tumor necrosis factor therapy is not associated with post-operative infection: results from prospective cohort of ulcerative colitis and Crohn's disease patients undergoing surgery to identify risk factors for postoperative infection I (Puccini). Gastroenterology 2019;156:S-80.

Conesa A, Madrigal P, Tarazona S, Gomez-Cabrero D, Cervera A, McPherson A, et al. A survey of best practices for RNA-seq data analysis [published correction appears in Genome Biol 2016;17:181]. Genome Biol 2016;17:13.

Contreras MA, Macaya L, Neira P, Camacho F, González A, Acosta J, et al. New insights on the interaction mechanism of rhTNFα with its antagonists adalimumab and etanercept. Biochem J 2020;477:3299–311.

Demichev V, Messner CB, Vernardis SI, Lilley KS, Ralser M. DIA-NN: neural networks and interference correction enable deep proteome coverage in high throughput. Nat Methods 2020;17:41–4.

Dobin A, Davis CA, Schlesinger F, Drenkow J, Zaleski C, Jha S, et al. STAR: ultrafast universal RNA-seq aligner. Bioinformatics 2013;29:15–21.

Dunn L, Prosser HC, Tan JT, Vanags LZ, Ng MK, Bursill CA. Murine model of wound healing. J Vis Exp 2013;75:e50265.

Eming SA, Krieg T, Davidson JM. Inflammation in wound repair: molecular and cellular mechanisms. J Invest Dermatol 2007;127:514–25.

Garg A, Birabaharan M, Strunk A. Prevalence of type 2 diabetes mellitus among patients with hidradenitis suppurativa in the United States. J Am Acad Dermatol 2018;79:71–6.

Gierek M, Klama-Baryła A, Łabuś W, Bergler-Czop B, Pietrauszka K, Niemiec P. Platelet-rich plasma and acellular dermal matrix in the surgical treatment of hidradenitis suppurativa: a comparative retrospective study. J Clin Med 2023;12:2112.

Gold DA, Reeder VJ, Mahan MG, Hamzavi IH. The prevalence of metabolic syndrome in patients with hidradenitis suppurativa. J Am Acad Dermatol 2014;70:699–703.

Gupta AK, Studholme C. Adalimumab (Humira) for the treatment of hidradenitis suppurativa. Skin Therapy Lett 2016;21:1–4.

Gurtner GC, Werner S, Barrandon Y, Longaker MT. Wound repair and regeneration. Nature 2008;453:314–21.

Huard J, Li Y, Fu FH. Muscle injuries and repair: current trends in research. J Bone Joint Surg Am 2002;84:822–32.

Jin L, Bi Y, Hu C, Qu J, Shen S, Wang X, et al. A comparative study of evaluating missing value imputation methods in label-free proteomics. Sci Rep 2021;11:1760.

Kelly G, Hughes R, McGarry T, van den Born M, Adamzik K, Fitzgerald R, et al. Dysregulated cytokine expression in lesional and nonlesional skin in hidradenitis suppurativa. Br J Dermatol 2015;173:1431–9.

Kimball AB, Okun MM, Williams DA, Gottlieb AB, Papp KA, Zouboulis CC, et al. Two phase 3 trials of adalimumab for hidradenitis suppurativa. N Engl J Med 2016;375:422–34.

Kohno T, Tam LT, Stevens SR, Louie JS. Binding characteristics of tumor necrosis factor receptor-Fc fusion proteins vs anti-tumor necrosis factor mAbs. J Investig Dermatol Symp Proc 2007;12:5–8.

Krzyszczyk P, Schloss R, Palmer A, Berthiaume F. The role of macrophages in acute and chronic wound healing and interventions to promote pro-wound healing phenotypes. Front Physiol 2018;9:419.

Larouche J, Sheoran S, Maruyama K, Martino MM. Immune regulation of skin wound healing: mechanisms and novel therapeutic targets. Adv Wound Care (New Rochelle) 2018;7:209–31.

Liao Y, Wang J, Jaehnig EJ, Shi Z, Zhang B. WebGestalt 2019: gene set analysis toolkit with revamped UIs and APIs. Nucleic Acids Res 2019;47:W199–205.

Lim SYD, Oon HH. Systematic review of immunomodulatory therapies for hidradenitis suppurativa. Biologics 2019;13:53–78.

Maarouf M, Clark AK, Lee DE, Shi VY. Targeted treatments for hidradenitis suppurativa: a review of the current literature and ongoing clinical trials. J Dermatolog Treat 2018;29:441–9.

Mitoma H, Horiuchi T, Tsukamoto H, Ueda N. Molecular mechanisms of action of anti-TNF-alpha agents - Comparison among therapeutic TNF-alpha antagonists. Cytokine 2018;101:56–63.

Moosvi Z, Abadir A, Duong J, Nguyen D. Q: Is it safe to continue biologic agents during surgery in patients with inflammatory bowel disease? Cleve Clin J Med 2020;87:343–6.

Murray PJ, Wynn TA. Protective and pathogenic functions of macrophage subsets. Nat Rev Immunol 2011;11:723–37.

Park Y, Yang J, Zhang H, Chen X, Zhang C. Effect of PAR2 in regulating TNF-alpha and NAD(P)H oxidase in coronary arterioles in type 2 diabetic mice. Basic Res Cardiol 2011;106:111–23.

Rennekampff HO, Hansbrough JF, Kiessig V, Doré C, Sticherling M, Schröder JM. Bioactive interleukin-8 is expressed in wounds and enhances wound healing. J Surg Res 2000;93:41–54.

Ring HC, Maul JT, Yao Y, Wu JJ, Thyssen JP, Thomsen SF, et al. Drug survival of biologics in patients with hidradenitis suppurativa. JAMA Dermatol 2022;158:184–8.

Ritchie ME, Phipson B, Wu D, Hu Y, Law CW, Shi W, et al. limma powers differential expression analyses for RNA-sequencing and microarray studies. Nucleic Acids Res 2015;43:e47.

Ritsu M, Kawakami K, Kanno E, Tanno H, Ishii K, Imai Y, et al. Critical role of tumor necrosis factor-α in the early process of wound healing in skin. J Dermatol Dermatol Surg 2017;21:14–9.

Robinson MD, Oshlack A. A scaling normalization method for differential expression analysis of RNA-seq data. Genome Biol 2010;11:R25.

Rodrigues M, Kosaric N, Bonham CA, Gurtner GC. Wound healing: a cellular perspective. Physiol Rev 2019;99:665–706.

Sabat R, Jemec GBE, Matusiak Ł, Kimball AB, Prens E, Wolk K. Hidradenitis suppurativa. Nat Rev Dis Primers 2020;6:18.

Saint-Georges V, Peternel S, Kaštelan M, Brajac I. Tumor necrosis factor antagonists in the treatment of pyoderma gangrenosum, acne, and suppurative hidradenitis (PASH) syndrome. Acta Dermatovenerol Croat 2018;26:173–8.

Sand FL, Thomsen SF. Off-label use of TNF-alpha inhibitors in a dermatological university department: retrospective evaluation of 118 patients. Dermatol Ther 2015;28:158–65.

Sandhu VK, Alavi A. The role of anti-tumour necrosis factor in wound healing: A case report of refractory ulcerated necrobiosis lipoidica treated with adalimumab and review of the literature. SAGE Open Med Case Rep 2019;7:2050313X19881594.

Santora LC, Kaymakcalan Z, Sakorafas P, Krull IS, Grant K. Characterization of noncovalent complexes of recombinant human monoclonal antibody and antigen using cation exchange, size exclusion chromatography, and Biacore. Anal Biochem 2001;299:119–29.

Savage KT, Flood KS, Porter ML, Kimball AB. TNF-alpha inhibitors in the treatment of hidradenitis suppurativa. Ther Adv Chronic Dis 2019;10:2040622319851640.

Sawaya AP, Stone RC, Mehdizadeh S, Pastar I, Worrell S, Balukoff NC, et al. FOXM1 network in association with TREM1 suppression regulates NET formation in diabetic foot ulcers. EMBO Rep 2022;23:e54558.

Shen S, Wang X, Zhu X, Rasam S, Ma M, Huo S, et al. High-quality and robust protein quantification in large clinical/pharmaceutical cohorts with IonStar proteomics investigation. Nat Protoc 2023;18:700–31.

Smith RA, Kirstein M, Fiers W, Baglioni C. Species specificity of human and murine tumor necrosis factor. A comparative study of tumor necrosis factor receptors. J Biol Chem 1986;261:14871–4.

Stekhoven DJ, Bühlmann P. MissForest–non-parametric missing value imputation for mixed-type data. Bioinformatics 2012;28:112–8.

Takeo M, Lee W, Ito M. Wound healing and skin regeneration. Cold Spring Harb Perspect Med 2015;5:a023267.

Theocharidis G, Thomas BE, Sarkar D, Mumme HL, Pilcher WJR, Dwivedi B, et al. Single cell transcriptomic landscape of diabetic foot ulcers. Nat Commun 2022;13:181.

Tran BN, Chan SL, Ng C, Shi J, Correia I, Radziejewski C, et al. Higher order structures of adalimumab, infliximab and their complexes with TNFα revealed by electron microscopy. Protein Sci 2017;26:2392–8.

Wang X, Jin L, Hu C, Shen S, Qian S, Ma M, et al. Ultra-high-resolution IonStar strategy enhancing accuracy and precision of MS1-based proteomics and an extensive comparison with state-of-the-Art SWATH-MS in large-cohort quantification. Anal Chem 2021;93:4884–93.

Xia J, Swiercz JM, Bañón-Rodríguez I, Matković I, Federico G, Sun T, et al. Semaphorin-plexin signaling controls mitotic spindle orientation during epithelial morphogenesis and repair. Dev Cell 2015;33:299–313.

Xu F, Zhang C, Graves DT. Abnormal cell responses and role of TNF-α in impaired diabetic wound healing. BioMed Res Int 2013;2013:754802.

Yan C, Grimm WA, Garner WL, Qin L, Travis T, Tan N, et al. Epithelial to mesenchymal transition in human skin wound healing is induced by tumor necrosis factor-alpha through bone morphogenic protein-2. Am J Pathol 2010;176:2247–58.

Zagaria O, Ruggiero A, Fabbrocini G, Gallo L, Romanelli M, Marasca C. Wound care, adalimumab, and multidisciplinary approach in a patient affected by PASH syndrome. Int Wound J 2020;17:1528–31.

Zouboulis CC, Okun MM, Prens EP, Gniadecki R, Foley PA, Lynde C, et al. Long-term adalimumab efficacy in patients with moderate-to-severe hidradenitis suppurativa/acne inversa: 3-year results of a phase 3 open-label extension study. J Am Acad Dermatol 2019;80:60–9.e2.